World Journal of Applied Chemistry
2021; 6(3): 25-35
http://www.sciencepublishinggroup.com/j/wjac
doi: 10.11648/j.wjac.20210603.11
ISSN: 2637-5966 (Print); ISSN: 2637-5982 (Online)

Enhanced Electro-optical Properties of Low Viscous Nematic Liquid Crystal Doped with Mixed Phase Anatase/Rutile TiO_2 Nanoparticles for Display Applications

Bhupendra Pratap Singh[1], Samiksha Sikarwar[2], Abhishek Kumar Misra[3], Pankaj Kumar Tripathi[1], Atul Kumar Srivastava[1], Meeta Sah[4], Rajiv Manohar[1, *], Kamal Kumar Pandey[4, *]

[1]Liquid Crystal Research Lab, Department of Physics, University of Lucknow, Lucknow, India

[2]Department of Physics, Babasaheb Bhimrao Ambedkar University, Lucknow, India

[3]Department of Physics, Government Vishwanath Yadav Tamaskar Post-Graduate Autonomous College, Durg, Chhattisgarh, India

[4]Shri Jai Narain Misra Post-Graduate College (KKC), Charbagh, Lucknow, India

Email address:

rajiv.manohar@gmail.com (R. Manohar), kamalpande27@gmail.com (K. K. Pandey)

[*]Corresponding author

To cite this article:

Bhupendra Pratap Singh, Samiksha Sikarwar, Abhishek Kumar Misra, Pankaj Kumar Tripathi, Atul Kumar Srivastava, Meeta Sah, Rajiv Manohar, Kamal Kumar Pandey. Enhanced Electro-optical Properties of Low Viscous Nematic Liquid Crystal Doped with Mixed Phase Anatase/Rutile TiO_2 Nanoparticles for Display Applications. *World Journal of Applied Chemistry*. Vol. 6, No. 3, 2021, pp. 25-35.
doi: 10.11648/j.wjac.20210603.11

Received: June 13, 2021; **Accepted**: June 28, 2021; **Published**: July 6, 2021

Abstract: Organic–inorganic composite based on liquid crystalline and TiO_2 nanoparticles were obtained and investigated taking into account the crystallographic form of TiO_2 i.e., anatase/rutile mixed phase. TiO_2 is an important class of material having various dielectric and electro-optical properties. The existent research presents the electro-optical properties of nematic liquid crystal (NLC) E204 and TiO_2 nanocomposites over an extensive range of frequencies. Various important display parameters such as response time, threshold voltage, pretilt angle and activation energy of pristine as well as TiO_2 doped composites systems were measured and analyzed. In comparison with the pure, TiO_2-doped composite systems has approximately 50% faster response time, owing to its remarkable decline in the relaxation time and activation energy of the LCs. The alteration in the optical intensity of the NLC composites as a function of the concentration of TiO_2 nanoparticles (NPs) was also examined. It was established that the optical intensity in nano-nematic composites was decreasing with the concentration of TiO_2 NPs. Also, it was observed that an escalation in the TiO_2 NPs concentration in NLC composites indicates to an escalation in the birefringence. Probable mechanisms of the interactivity between NLC molecules and TiO_2 NPs have been discussed. The current work shows that the TiO_2 NPs doping has an encouraging application in the display devices, including other electro-optical as well as photonic applications.

Keywords: Liquid Crystal, Response Time, Pretilt Angle, Threshold Voltage, Birefringence, Activation Energy

1. Introduction

Liquid Crystals (LCs) are composed of moderate size organic molecules having properties between solids and liquids. This is a strange form of matter which generated the curiosity in scientists of the previous century. They are extensively used in industries with wide range of applications which is still growing. LCs are classified in broad categories but it is mostly thermotropic liquid crystal (LC) that are used in photonic applications. The LCs in which phase transitions occur due to change in temperature are called thermotropic [1] Liquid crystalline materials, themselves being a blend of crystalline solids and isotropic liquids lead one into the heartland of interdisciplinary science where organic chemistry, physics and material science meet. Nematic phase of liquid crystals has bagged ample focus because of its widespread scope both in

fundamental science and its applications. The rod-like simple structure of this liquid crystalline phase has made it the first choice of researchers around the globe. Nanoparticle-LC composite system, as a subject area has arisen from the interaction of two well-established sciences. One is liquid crystal science that has observed a tremendous upsurge of interest due to its application in display devices which in turn has fueled it with funds and new challenges. Nanomaterial science, comparatively, is somewhat younger but has marked its presence as of new materials with novel processing capabilities and with the prospect of unique combinations of properties. The amalgamation of LCs with nanomaterials is of emerging concern for the soft condensed matter researcher and has been studied widely in the recent years [2-4]. In the literature, there are acceptable confirmations according to which doped NPs enhance the properties of host LCs [5-7]. A lot of exertions have been put to enhance the properties of LCs by dispersion of various metal NPs such as gold nanoparticles (GNPs) [8-14], silver nanoparticles (Ag NPs) [15-19], dyes [20-22], TiO_2 NPs [23-26] quantum dots (QDs) [27, 28], carbon nanotubes (CNTs) [29, 30], polymers [31, 32] and nanorods [33-35].

Titanium dioxide (TiO_2) is an important material for various technological applications. It has gained considerable attention in device applications. The vast permittivity and refractive index, non-toxicity, chemical inertness and potential photocatalytic activity of TiO_2 NPs have made it a great candidate for photonic applications (especially for Guest-Host interactions). Generally, three distinct polymorphs of TiO_2 exist in the nature, which are anatase, rutile (both tetragonal crystal systems) and brookite (orthorhombic crystal system). Among these, anatase phase exhibits best photocatalytic properties, followed by rutile and brookite. Under comprehensive conditions, macrocrystalline rutile phase is thermodynamically more stable than anatase and brookite. In the ambient environment, the average particle size of anatase phase is below 11 nm, brookite phase is between 11 nm to 35 nm and rutile phase is above 35 nm [36]. In guest-host applications anatase phase is extensively castoff as a dopant material in LC investigations due to its high optical activity. For instance, the photoluminescence (PL) intensity of the anatase TiO_2 NPs doped with antiferroelectric liquid crystal (AFLC) materials has been augmented due to constructive combined emissions from TiO_2 NPs and AFLC as they have conjoint wavelength span in their emission bands [37]. C. Y. Huang et al. [38] Examined silane coated anatase TiO_2 NPs in high dielectric anisotropic nematic LC and found suppressed screen effect, decreased threshold and driving voltage, also decreased order parameter. P. C. Wu et al. [39] found suppressed ionic effect and promoted voltage holding ratio (VHR). Moreover, H. Ayeb et al. [40] reported about 5% enhancement in order parameter by the dispersion of pure and copper doped TiO_2 NPs in 5CB LC. It is worth to notice that the assorted phase of anatase/rutile TiO_2 nanoparticles is a reliable candidate to fabricate high performance display devices owing to its extraordinary photocatalytic activity, refractive index, dielectric constant and optical activity [41]. So, by espousing a well-judged combination of anatase/rutile phase of TiO_2 NPs exciting results in the LC can be acquired. However, the electro-optical and dielectric properties of mixed phase anatase/rutile TiO_2 NPs present in the low viscous nematic LC have been reported rarely in literature.

Herein, we examined E204, a low viscous nematic liquid crystal, doped with mixed phase anatase/rutile TiO_2 nanoparticles. Different concentration of TiO_2 NPs has been used to quantify electro-optical characteristics for the enhancement of various display properties. The TiO_2 NPs have a reduced dimension with superior aspect ratio; therefore, they play the key role in enhancing many catalysis activities. TiO_2 NPs have engrossed sufficient consideration as proficient application in LC devices because they have high permittivity and refractive index, with non-toxic and chemical inert nature. Also, they are highly cost effective. To explain the faster response time, the physical properties of NLCs have been quantified. Herein, the influence of doping TiO_2 NPs on the display characteristics of nematic liquid crystal (NLC) which can perturb the dynamic response time, dielectric anisotropy, threshold voltage and pretilt angle have been stated. The birefringence of pure and dispersed LCs has been described. The significant reduction in the transmission intensity has been detected in the TiO_2 doped LC cell. The voltage dependent transmission spectra have been used to estimate the threshold voltage of pristine and doped LC cells. Dielectric spectra of the TiO_2 doped LC cells have also been quantified to identify the dielectric anisotropy of LCs. The pretilt angle of the molecules out of the plane of the glass plate is obtained as a function of the applied voltage. It was analyzed that TiO_2 NPs doping descents the order parameter. Then it can be estimated that TiO_2-doped LC cell has conveyed nearly two-fold faster response time than the intrinsic one.

2. Materials and Methods

A mercantile NLC material, namely, E204 (BDH Chemicals Ltd, UK) was employed in contemporary research. The host BDH mixture E204 is a low-viscous mixture with extensive functioning temperature range based on fluorobiphenyl component. The E204 has positive dielectric anisotropy ($\Delta\varepsilon$) 6.4 at 1kHz, clearing point 89.8°C, viscosity 24.8 centistokes (cSt) at 20°C and the optical birefringence (Δn) of the LC at 589 nm and 20°C was 0.142 [42]. In this study, TiO_2 NPs with rutile phase (Sky Spring Nanomaterials, Inc., USA) were used as a guest material. The rutile and anatase phase of TiO_2 NPs have the dielectric constant 86 to 170 (depending on the crystal rotation) and ~40 respectively [43]. The average dimension of the NPs was ~40 nm, much less than the wavelength of visible light hence inhibited the optical scattering properties.

2.1. Experimental Details and Measurement Techniques

This section includes the instruments and experimental procedures castoff in the investigation. Scanning electron microscopy (SEM) was done using Quanta 200 which revealed the morphology of nanoparticles. X-ray diffraction (XRD) was executed by exhausting X-ray diffractometer

Rigaku Miniflex 600 with control voltage/current of 20 kV/ 2 mA (under XG operation) using CuK_α radiation (1.54 Å) and 2θ ranging from 20° to 80°. The dielectric properties of pure and doped LC cells were quantified using an LCR meter (Hioki 3532-50, Nagano Prefecture, Japan). The applied field (AC) to the cell was 0.01 V/µm whereas frequency was diversified from 42 Hz - 5.5 MHz. Further, dielectric permittivity (ε′) and dielectric loss (ε′) respectively were obtained from the relations given in equations (1) and (2):

$$\varepsilon^{'} = \frac{C_p d}{\varepsilon_o A} \tag{1}$$

$$\varepsilon^{''} = \frac{d}{2\pi f \varepsilon_o A R_p} \tag{2}$$

Here, C_p = capacitance,
d = cell thickness,
A = active surface and
R_p = resistance of LC layer

The pre-tilt angles of doped cells were quantified by employing the crystal rotation technique [44]. The voltage-transmittance (T-V curve) of the intrinsic and doped cells were obtained by exhausting self-designed experimental setup wherein a 10 mW He-Ne laser (wavelength 632.8 nm) was incident perpendicularly on the sample cell which was mitigated by the ND filter. The waveform of the applied voltage was square wave having frequency 1 kHz. The sample cell was located between a pair of crossed polarizers in such a way that it forms an angle of 45° along the transmission axis of the polarizer and the rubbing direction of the cell. The response time was obtained by optical switching method for the intrinsic and nano-nematic complexes [14]. The relationships among fall time (τ_{off}), rise time (τ_{on}), threshold voltage (V_{th}) and rotational viscosity (γ) is discerned by the equations 3-5 when the applied voltage (V_{app}) is much higher than V_{th} [45].

$$\tau_o = \frac{\gamma d^2}{K_{11}\pi^2} \tag{3}$$

$$\tau_{on} = \frac{\tau_o}{\left|(\frac{V_{app}}{V_{th}})^2 - 1\right|} \tag{4}$$

$$\tau_{off} = \frac{\tau_o}{\left|(\frac{V_{bios}}{V_{th}})^2 - 1\right|} \tag{5}$$

Here τ_0 denotes the relaxation time constant when the LC cell is turned off from V_{app} slightly higher than V_{th}, K_{11}, V_{bias} and d represents the splay elastic constant, bias voltage and cell thickness respectively. The τ_{on} / τ_{off} is the time required for the maximum transmittance intensity to change from 10% to 90% and 90% to 10% respectively. For τ_{on}, the voltage rises from 2.5 V to 10 V whereas for τ_{off}, it falls from 10 V to 2.5 V.

The birefringence (Δn) of LC is a mesmerizing characteristic owing to its essential significance in LC devices. The birefringence (Δn) is defined as the difference between extra-ordinary (n_e) and ordinary (n_o) components of the refractive index of material. The details about birefringence measurement are given in reference [14, 46]. The optical birefringence of weakly polar nematic and TiO_2 NPs doped composites has been obtained by equation 6.

$$\Delta\phi = \frac{2\pi d \Delta n}{\lambda} \tag{6}$$

Here, $\Delta\phi$ = phase difference,
d = cell thickness,
λ = wavelength of He-Ne laser.

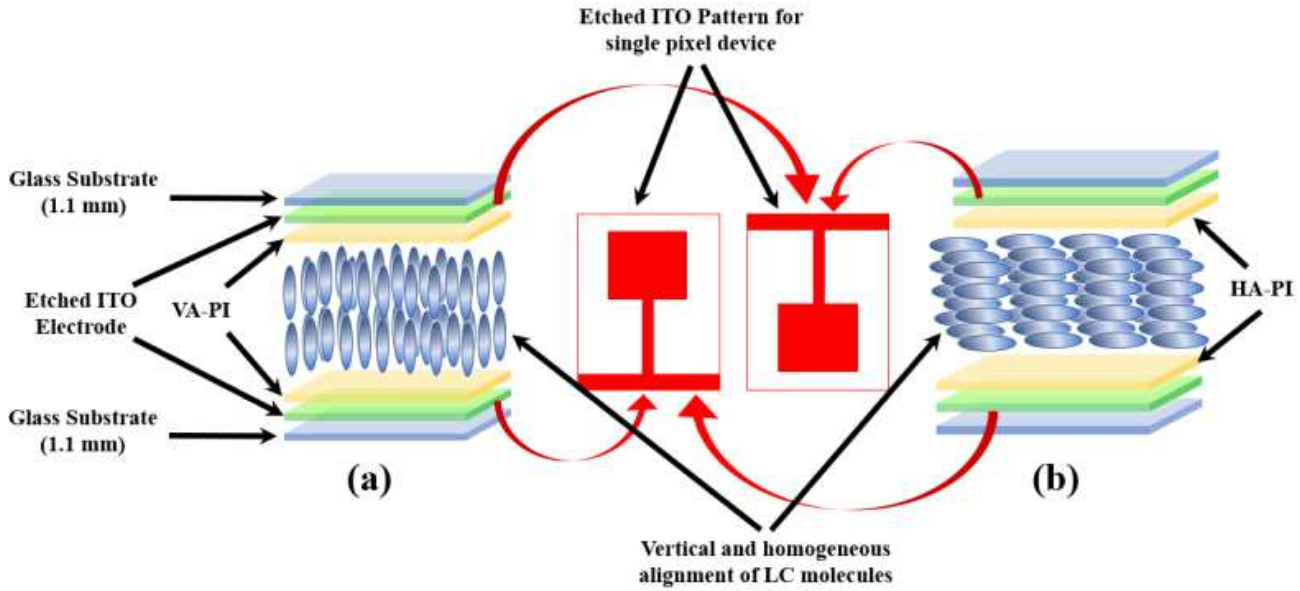

Figure 1. *Structure of the sample cell (single pixel) (a) Vertical aligned and (b) Homogeneously aligned LC cells used in the present investigation.*

2.2. Sample Cells Preparation

Commercially obtainable optically flat indium tin oxide (ITO) substrates were employed as electrodes for the fabrication of sample cells. These ITO substrates have transmittance more than 90% and resistance 10 Ω/mm^2 (Chipset Technology Co. Ltd., Miaoli, Taiwan). A homogeneous layer of negative photoresist (NPR) onto the conducting surface of the well cleaned glass substrates by spin coating technique was deposited. Further, these substrates were placed on the hotplate at 100°C for 3 min. Then, the photomask of desired pattern was applied on the plates and they were exposed to the UV light for 100 s. The substrates were then dipped in developer (~40 ml) for 40 s and washed with reverse osmosis (RO) water and kept on the hotplate for 5 min. Further, these plates were dipped in etchant containing beaker at 60°C for 120 s. These plated were then washed with RO water followed by acetone and kept in oven at 80°C for 20 min and 200°C for 80 min. Finally, the baked substrates were subjected to antiparallel rubbing treatment, assembled by using 6 µm mylar spacer between them and sealed with glue. Finally, the width was inveterate by optical interferometric technique to be ~6.1±0.05 µm. The material was filled into the cell with capillary action above the isotropic temperature of the material. The proper alignment of the LC molecules was tested by placing the sample cell under the crossed position of the optical polarizing microscope (POM) as shown in Figure 1 [24].

3. Results and Discussion

Figure 2 (a and b) shows the Scanning Electron Microscope (SEM) image and X-ray diffraction (XRD) pattern of TiO_2 NPs. SEM analysis confirms that the NPs are almost spherical in shape with average diameter of ~40 nm. XRD reveals the crystal nature of the material. Both the position and intensity of lines in the X-ray spectrum are characteristic of the particular phase and provide a fingerprint of the material. Peaks of the rutile phase corresponding to (110), (101), (111), and (220) planes appear at 27.37°, 36.02°, 41.16°, 56.53° respectively and confirms the of the rutile phase of the material as compared from the standard data (JCPD card no. 77-0441). Crystallite size was estimated using Scherrer's formula given in equation 7.

$$P = \frac{0.89\lambda}{\beta_{1/2}\cos\theta} \tag{7}$$

Here, λ, θ and $\beta_{1/2}$ represents the wavelength of X-ray, Bragg's angle and full-width at half maximum (FWHM) intensity respectively. The assessed crystallite size of the NPs was found in the range ~35 to 40 nm which is consistent with the size asserted by the supplier.

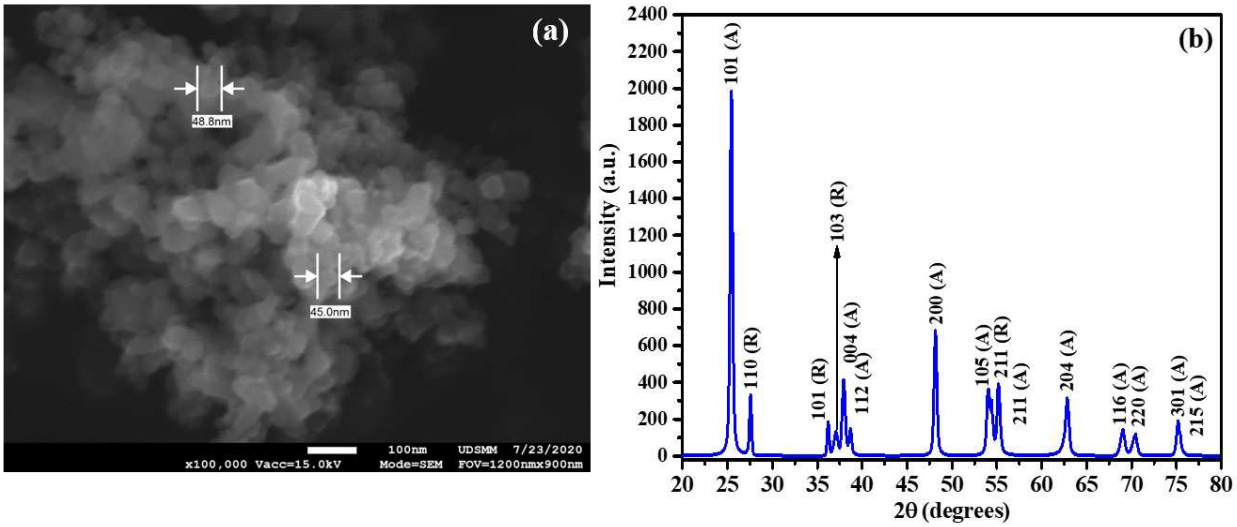

Figure 2. *(a) Scanning electron microscopic (SEM) image and (b) X-ray diffraction pattern of the TiO_2 NPs. The abbreviations A and R represent the anatase and rutile phases, respectively.*

Figure 3 depicts the dielectric spectra of homogeneously-aligned (HA) and vertically-aligned (VA) TiO_2-doped LC cells. Figure 2 (a and b) epitomizes the deviation of perpendicular and parallel component of dielectric permittivity ($\varepsilon'_{\perp}$ and $\varepsilon'_{\parallel}$) analogous to frequency for intrinsic E204 and doped LC cells at room temperature (RT). Here, two fascinating factors have been observed, viz.: (i) TiO_2 doping upsurges the permittivity (ε') and dielectric loss (ε'') of both (HA & VA) LC cells; (ii) Dielectric anisotropy ($\Delta\varepsilon = \varepsilon_{\parallel} - \varepsilon_{\perp}$) appears to decrease slightly with rise in the amount of TiO_2. In the HA cell, the LC molecules are located parallel to the glass plates. Therefore, normal to the direction of applied electric field. Similarly, in the VA cell, LC molecules are oriented perpendicular to the substrate hence parallel to the direction of applied electric field. An externally applied electric field to the dielectric medium takes the system to the new equilibrium state through dielectric relaxation. Dielectric relaxation is accredited to the reason that electric displacement necessitates a fixed time to attain the equilibrium. Since on ITO electrode, finite resistance of the LC cell and the inductance of the copper tape can also influence the relaxation mode significantly, subsequently, for

the endorsement of relaxation mode of the LC cells, the dielectric spectra of the empty cell were also quantified and found that the relaxation mode of the empty cell is at ~10 MHz at RT. Notably, the relaxation frequency is sturdily reliant on temperature. These relaxation times are related with the molecular polarization rotation time around the short or long molecular axis of NLCs [47].

The relaxation frequency of HA cell was detected at 2.74, 3.00, 2.68 and 2.80 MHz and for VA cell at 0.70, 0.76, 0.88 and 1.10 MHz for pristine E204, 0.1 wt%, 0.5 wt% and 1.0 wt% TiO_2 concentration respectively (Figure 3 (a) and 3 (b)). The relaxation frequency ($f^{\parallel}$) of VA cell is slightly lower than the relaxation frequency of HA cell ($f^{\perp}$); i.e. the relation $\tau = 1/2\pi f$ signifies that $\tau_{\parallel}$ of dielectric polarization is slower than the $\tau_{\perp}$ as shown in Figure 3. Where the relaxation frequency of NLCs is the peak frequency of dielectric loss. The $\tau_{\parallel}$ and $\tau_{\perp}$ correspond to molecular polarization times around the short and long molecular axis of NLCs [48]. In case of positive dielectric anisotropic NLC, polar substituents are used to induce the permanent molecular electric dipole moment, parallel to the long molecular axis of NLC molecules, so that the dielectric relaxation caused by polar substituents, corresponds to $\tau_{\parallel}$ term.

The frequency dependent dielectric loss and relaxation time of VA cell of TiO_2 NPs doped LC were quantified to ascertain the impact of TiO_2 NPs on the motion of NLC. The relaxation frequency of dielectric loss of VA cell (peak frequency $f_p^{\parallel}$) was moved towards higher frequency regime with the dispersion of TiO_2 NPs (Figure 3 (d)). This relaxation mode was subsequently associated with the short molecular axis of LC molecules reorientation. The relaxation time ($\tau_{\parallel}$) of the positive dielectric anisotropic NLCs can be associated with the relaxation frequency by $\tau_{\parallel}=1/2\pi f_p^{\parallel}$. The relaxation time is also linked with the potential barrier parameter (η) by using the expression η = b/RT, where b is the height of the potential barrier around the short molecular axis, R is the gas constant and T is the ambient temperature. Meier and Saupe found that η is proportional to the relaxation time [48]. In the present study, pure E204 has lower relaxation relative to the doped cells which correspond that doped LCs have faster relaxation time. Consequently, TiO_2 doping declines the height of the potential barrier around the short molecular axes of the LCs, thus drops the associated rotational viscosity (γ) of the system [49]. Which further escalates the response time of the TiO_2 dispersed system. Remarkably, the measured relaxation frequency of the LC layer should be smaller than that of exact relaxation frequency attributable to the impact of cell relaxation. The exact relaxation frequency of the LCs can be assessed by knowing the precise value of inductance of the copper tape and ITO resistance. The influence of TiO_2 on LCs can be detected and elucidated. Figure 3 (e) shows $\Delta\varepsilon$ (of pure and doped LCs) slightly reduces with increasing TiO_2 NPs concentration.

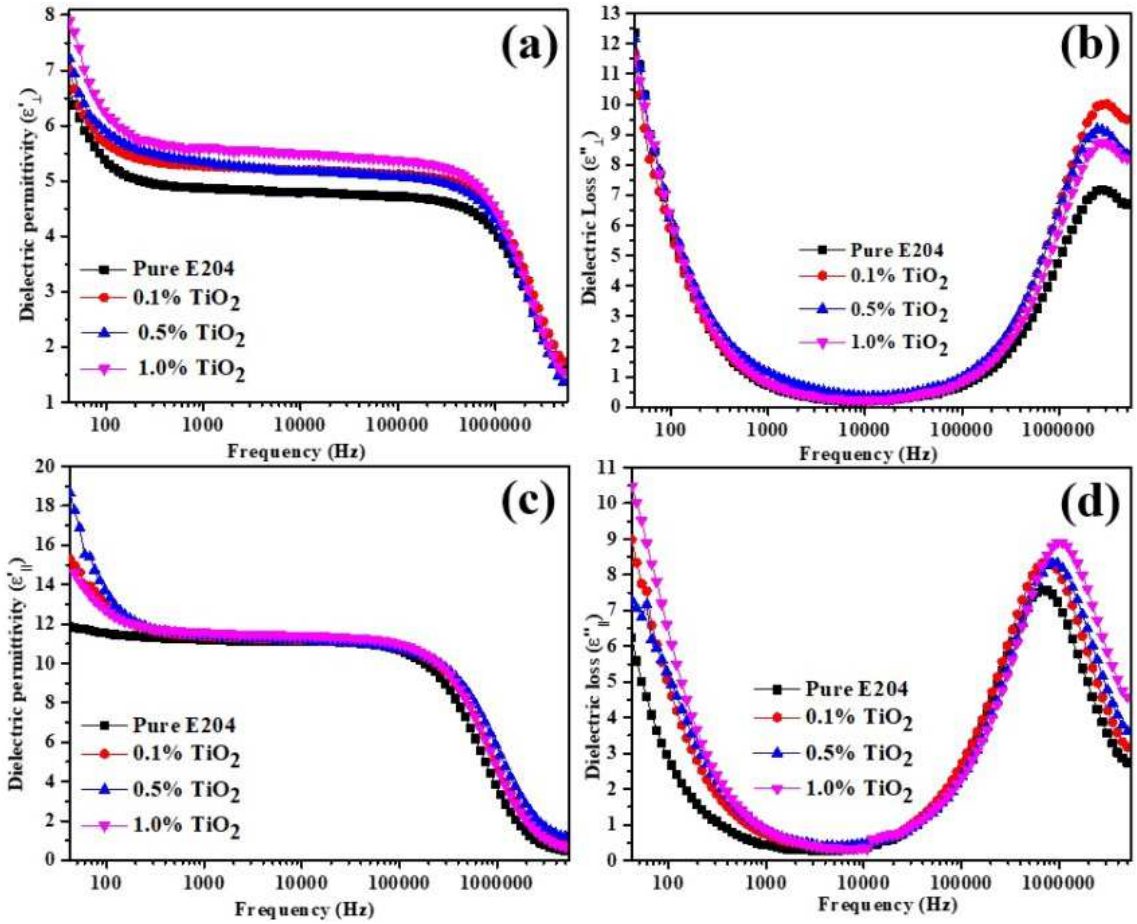

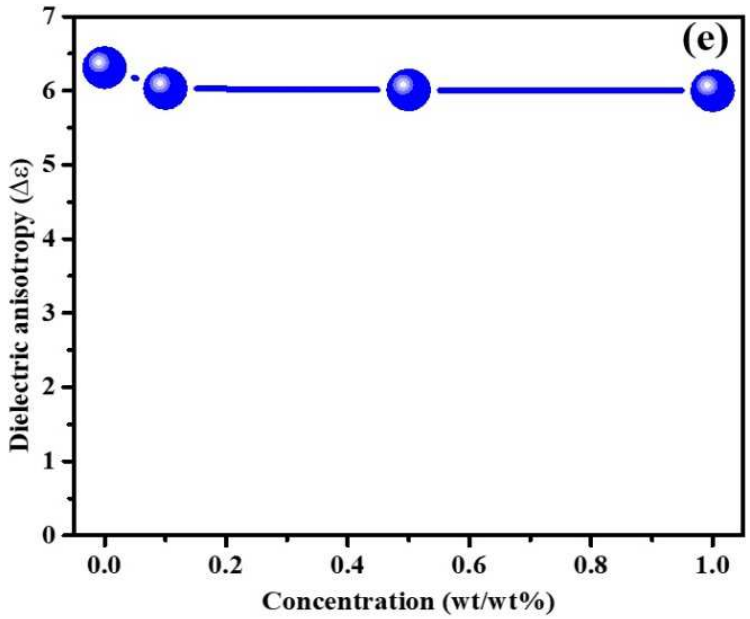

Figure 3. *Dielectric spectra of HA sample depicting (a) dielectric permittivity, (b) dielectric loss; VA sample showing (c) dielectric permittivity, (d) dielectric loss and (e) dielectric anisotropy of LC cells with various concentration of TiO_2 NPs.*

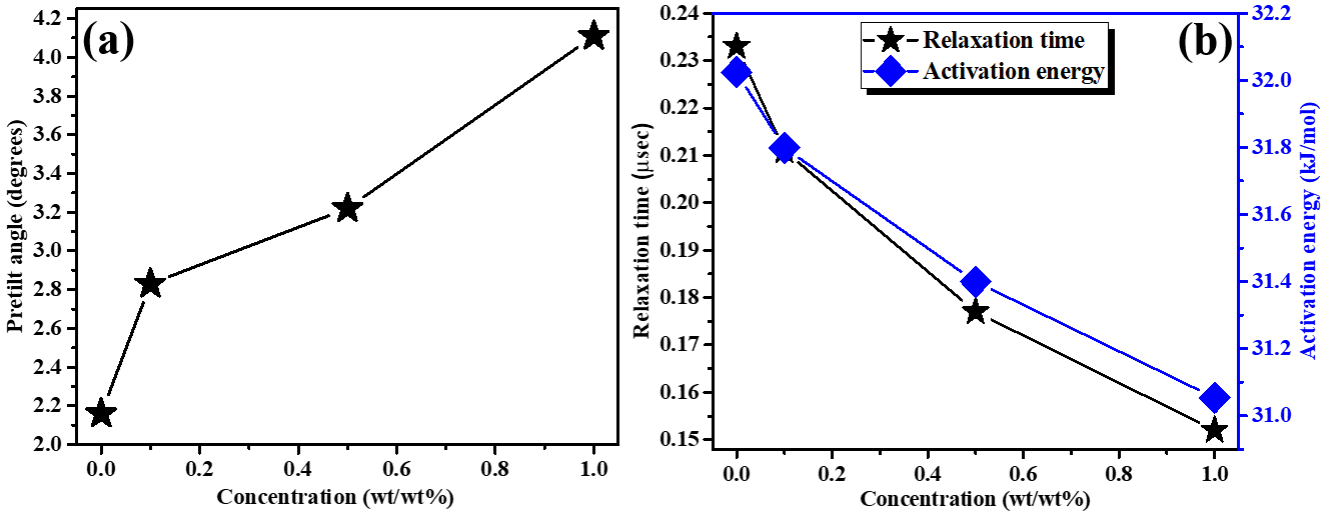

Figure 4. *Variation of (a) Pretilt angle and (b) relaxation time and activation energy of LC cells corresponding to TiO_2 NPs concentration.*

The pretilt angle of the LC cells doped with 0.1 wt% to 1.0 wt% TiO_2 NPs were analysed by crystal rotation method using the transmittance measurement [44]. The pretilt angles of pure E204, 0.1 wt%, 0.5 wt% and 1.0 wt% TiO_2 NPs doped samples were found 2.1°, 2.8°, 3.2° and 4.1° respectively as shown in Figure 4 (a). Numerous mechanisms have been studied to explain the pretilt angle [50]. The mechanism of change in pretilt angle has been explained ahead.

This phenomenon is due to the adsorption of NPs on the inner surface of LC cells [51, 52]. The adsorption of the NPs on the substrates mediated and lowered the surface tension of the substrates, subsequently modified the pretilt angle of LC molecules (Figure 4 (a)). The small amount of NPs allowed little increment in the pretilt angle from 2.1° to 4.1°. The relaxation time and activation energy followed the analogous trend as tilt angle but in opposite manner as shown in Figure 4 (b). The relaxation times of pure, 0.1 wt%, 0.5 wt% and 1.0 wt% TiO_2 NPs doped samples were 0.235 µs, 0.210 µs, 0.176 µs and 0.154 µs respectively. The adsorbing NPs on the surface of the substrate made it little bit easy to reorient the LC molecules in their vertical tilt position and this took less time to relax the doped LC molecules as compared to pure one. Activation energy analogous to TiO_2 NPs is also demonstrated in Figure 4 (b). The activation energies of pure, 0.1 wt%, 0.5 wt% and 1.0 wt% TiO_2 NPs doped samples were 0.227 KJ/mole, 0.210 KJ/mole, 0.181 KJ/mole and 0.165 KJ/mole respectively. The reduction in the anchoring energy was due to the downfall in the relaxation time. The activation energy diminished with the growing amount of NPs. The decrement in the value of activation energy means fast relaxation of the LC molecules. The fast relaxation of the LC molecules is accredited to the electric properties of spherical TiO_2 NPs as is explained further in the theory of response time [50-53].

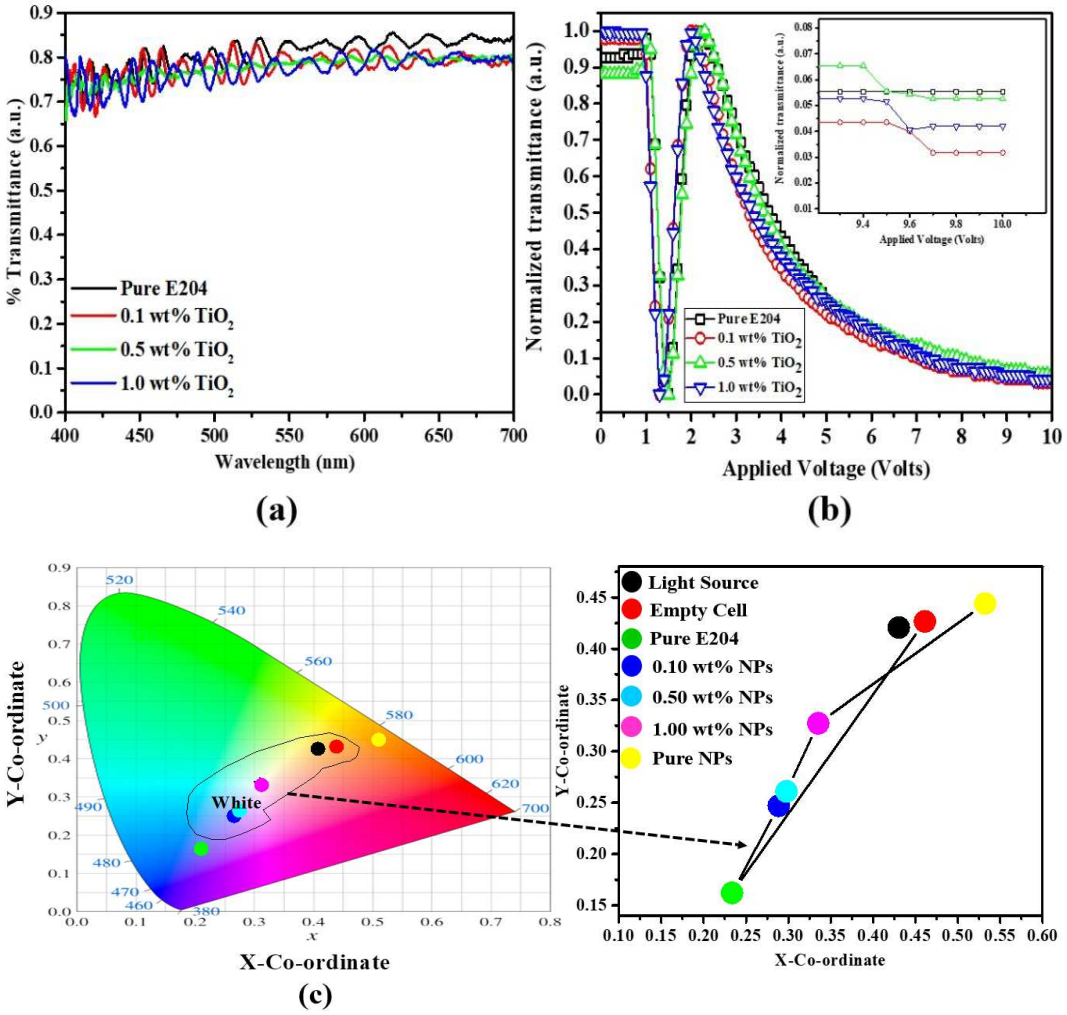

Figure 5. *(a) Transmission spectrum and (b) Voltage dependence of transmittance (T-V) curves and (c) CIE 1931 color chromaticity diagram of the NLC cells at different TiO_2 NPs doping concentration.*

Figure 5 (a) epitomizes the transmission spectra of the TiO_2-doped LC cells in the visible range of the electromagnetic spectrum (400 and 700 nm). The light loss of ~8% (dropped from 78% to 70%) occurred because TiO_2 doping altered the refractive index of LC mixture thus increasing the refractive index mismatch between the surfaces of glass substrates and LC layer. The voltage transmittance (T-V) curves of the intrinsic, 0.1 wt%, 0.5 wt% and 1.0 wt% TiO_2 NPs doped samples are epitomized in Figure 4 (b), which were then used to calculate the threshold voltage by transferring them into phase curves. As the applied electric field increased, the transmittance remained constant up to initial distortion in electrically controlled birefringence (ECB) mode of LC then it decreased rapidly to zero and increased rapidly to the driving voltage and then decreased until saturation threshold not reached. The voltage corresponding to 90% transmission in phase curves is demarcated as threshold voltage. The threshold voltage was found decreasing with increasing TiO_2 NPs doping concentration. The voltage at which the LC molecules starts rotating is called threshold voltage (V_{th}), which defines the minimum voltage required for the specific LC cell to work. The pure LC cell unveiled the highest value of threshold voltage 1.3 V while that of 0.1 wt%, 0.5 wt% and 1.0 wt% TiO_2 NPs doped samples were 1.0 V, 0.9 V and 0.8 V respectively, i.e. the threshold voltage reduced by 38 % approximately. Whereas, the decrease in the driving voltage (V_d) (~9%) was also detected by the dispersion of TiO_2 NPs. The T-V curve also demonstrates that the standard static contrast ratio (inset figure 5b) of the TiO_2 doped LC cells has been reduced as compared to pure E204 at 10 V. The reinforced electric field around the TiO_2 NPs with the LC director encouraged the electro-optical response by the dropping the threshold voltage (V_{th}) and driving voltage (V_d) of the LC mixture. The reduction in V_{th} occurred by the effective dielectric anisotropy ($\varepsilon_{NPs,\ LC} > \varepsilon_{LC}$) of the composite system, which turned in a larger torque for the blend ($\varepsilon_{NPs,\ LC}.\ E^2 > \varepsilon_{LC}.\ E^2$), instigating faster LC alignment. Locally oriented TiO_2 NPs have fundamental dipole moments and align very rapidly along the direction of the applied field, in turn driving a faster alignment of the TiO_2 doped mixture resulting in superior switching properties relative to the

intrinsic LC. Also, lowering of threshold voltage is an imperative prerequisite for conventional display devices, because it necessitates a diminution in power consumption. The field ‘‘on–off’’ electro-optical responses with TiO_2 NPs doped at various concentrations exhibited faster response times compared to pure E204 (Figure 6). The lower V_{th} and faster response time are essential from the outlook of applications of LC devices. Amalgamations of TiO_2 NPs with LCs might meet subcomponent fabrication criterions, and proposes manufacturing potentials with wide viewing angles and better contrast ratios and faster switching time.

Figure 5 (c) shows the Commission Internationale de ÍÉclairage (CIE) 1931 chromatographic coordinates’ diagram, which elucidates the stimuli-induced color transformation. The luminescence parameters entitles that the intensity and color of the luminescence faintly varies with the increase in TiO_2 NPs concentration, indicating TiO_2 NPs doping does result in color shifts of the LC cell because it has an absorbance in short wavelength region. The color shift lies on the black body locus on the chromaticity diagram which have its own technological importance in display industry.

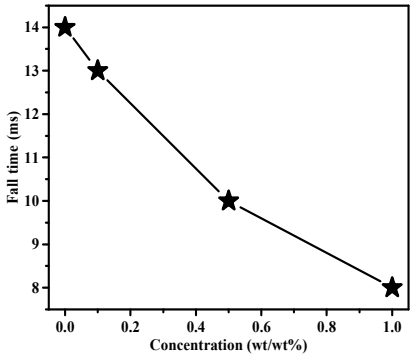

Figure 6. *Fall time of the NLC with various TiO_2 concentrations at RT.*

Table 1. *CIE color coordinates (x, y) of TiO_2 NPs -doped LC cell at RT.*

TiO_2 NPs Concertation (wt%)	x	y
Light Source	0.4302	0.4206
Empty Cell	0.4612	0.4266
Pure E7	0.2335	0.1622
Pure TiO_2 NPs	0.5322	0.4440
0.10	0.2887	0.2470
0.50	0.2978	0.2610
1.00	0.3352	0.3273

Figure 6 shows the fall time of the intrinsic and NPs doped LC analogous to the applied electric field for a planar aligned cell at RT. In this experiment, the rise time of the TiO_2-doped LC cells was approximately persistent to ~963 µs at RT, as a result of the same turn-on voltage. Remarkably, the fall time of TiO_2 doped LC cell decreased with growing TiO_2 concentration. The fall time of pure, 0.1 wt%, 0.5 wt% and 1.0 wt% TiO_2 NPs doped samples was found 14 ms, 13 ms, 10 ms and 8 ms respectively. The fastest response time (rise time + fall time) was observed for 1 wt% TiO_2 NPs doped LC.

The diminution in the response time and threshold voltage is explained here. Under an applied voltage, just outside the spherical NPs, the field is perpendicular and charge distribution takes place in such a way that it kills the tangential component of electric field. Because of the surface charge density of the TiO_2 NPs, they change the path of the electric field lines (as shown in Figure 7) which is known as spontaneous polarization electric field (SPEF). Near TiO_2 NPs, the electric field lines are more focused and hence electric field strength around the spherical NPs considerably increased. Due to this strong field, the LC molecules fall very quickly when the field goes to off. Hence this mechanism explains the lower threshold voltage and faster response time of TiO_2 NPs doped LC samples.

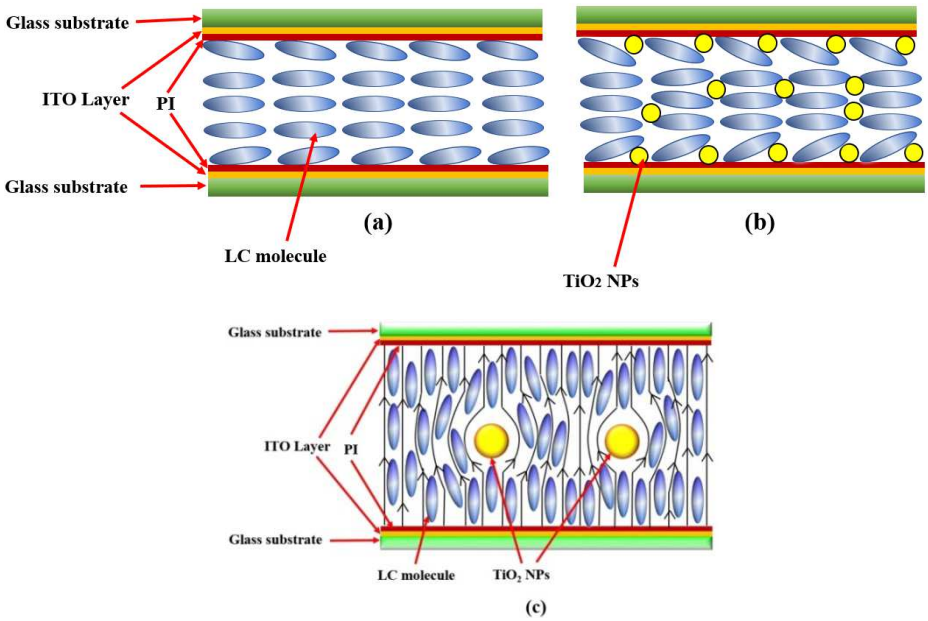

Figure 7. *The schematic diagram of molecular arrangement of NLC and NPs (a) normal pretilt due to anchoring energy of polyimide layer (b) enhancement of pretilt angle by adsorption of TiO_2 NPs on the substrate and (c) spontaneous polarization electric field (SPEF) of TiO_2 NPs to provide additional restoring force to the NLC media.*

Figure 8 demonstrates the alteration of birefringence (Δn) relative to temperature for intrinsic and TiO_2 NPs doped LCs at certain wavelength. The birefringence of pure, 0.1 wt%, 0.5 wt% and 1.0 wt% TiO_2 NPs doped samples was 0.155, 0.165, 0.175 and 0.185 respectively. The alteration of the birefringence reflecting the nature of local orientational order as well as refractive index mismatch between the surfaces of glass substrates and LC layer in the pure and NPs dispersed LCs. As explained in previous section that the TiO_2 doping modulates the refractive index of LC mixture and hence increases the refractive index mismatch among the surfaces between glass substrates and LC layer, therefore, the local orientation and refractive index mismatch attributes to the small increment in the birefringence [52].

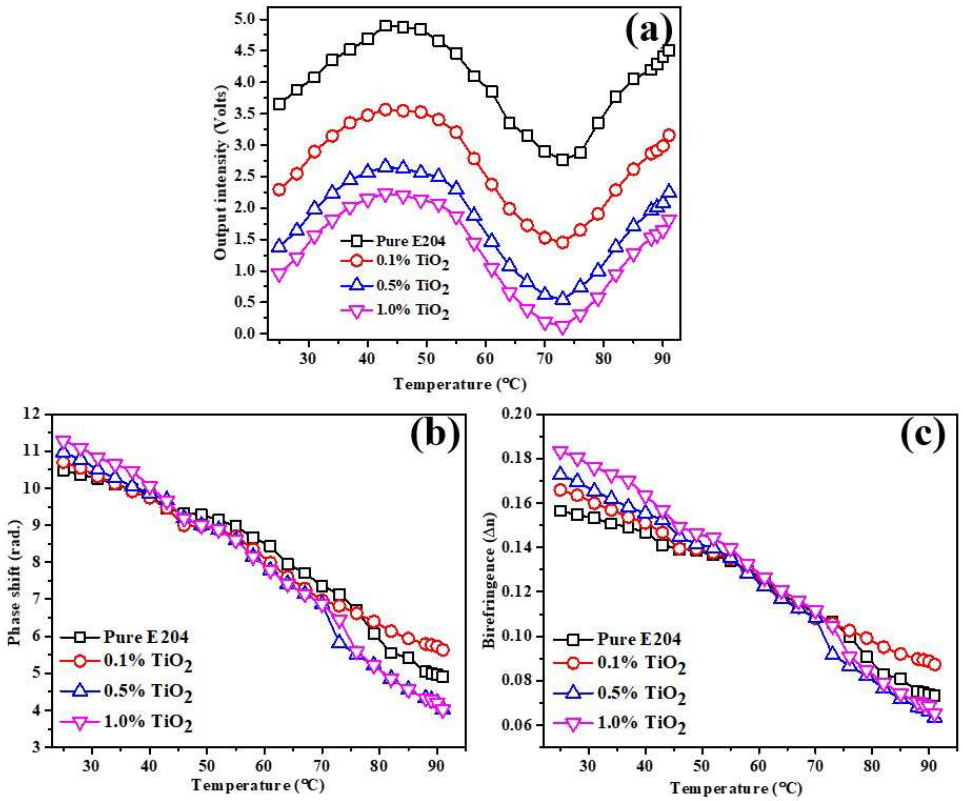

Figure 8. *Variation of (a) output intensity, (b) phase shift and (c) birefringence relative to temperature for intrinsic and doped LC.*

4. Conclusion

The influence of TiO_2 NPs on E204 LCs was explored in the current article. The strong interactivity between the TiO_2 NPs and LCs was endorsed by dielectric and electro-optical measurements. Moreover, TiO_2 doping reduced the activation energy (E) of the LC mixture, subsequently, the rotational viscosity (γ) of the system. Decrease in γ, accelerated the response time (nearly two-fold) of the TiO_2 dispersed system. The response time was also elaborated considering strong field near the LC molecules, due to which the molecules fell very quickly when the field goes off. The fast relaxation time (~36%) of the LC molecules was also described considering the electric parameters of spherical TiO_2 NPs. A little bit rise in the tilt angle was observed which might be because of the adsorption of NPs on the surface of the substrate. The local orientation and refractive index mismatch accredited to the small increment (~19%) in the birefringence. The present work revealed that TiO_2 NPs doping has a better application in the electro-optical as well as photonic applications. Future work involves the investigation of dielectric and electro-optical performances of LC-TiO_2 composite systems and optimization of threshold limit of the concentration by different dispersion methods such as by using different solvents and fine bead mill method for the optimization of best results for the development of better electro-optical devices.

Conflict of Interest

The authors declare that they have no competing interests.

Acknowledgements

The author B. P. Singh is sincerely thankful to the INSPIRE-AORC Program of the Department of Science & Technology (DST), New Delhi [No. DST/INSPIRE Fellowship/2016/IF160572] for providing financial assistance in the form of INSPIRE Fellowship. Author R. Manohar is thankful to UGC for 'MID CAREER AWARD' [No. F.19-224/2018 (BSR)]. Author A. K. Srivastava is thankful to state government Uttar Pradesh for the center of excellence project at A. P. J. Abdul Kalam Centre.

References

[1] D.-K. Yang, Wu, Shin-Tson, Wiley series in display technology 1 (2014) 259.

[2] E. Ouskova, O. Buchnev, V. Reshetnyak, Y. Reznikov, H. Kresse, Liquid Crystals 30 (2003) 1235.

[3] R. Basu, G. S. Iannacchione, Journal of Applied Physics 106 (2009) 124312.

[4] Neeraj, K. K. Raina, Phase Transitions 83 (2010) 615.

[5] S. W. Lee, C. Mao, C. E. Flynn, A. M. Belcher, Science 296 (2002) 892.

[6] M. Tamborra, M. Striccoli, R. Comparelli, M. L. Curri, A. Petrella, A. Agostiano, Nanotechnology 15 (2004) S240.

[7] E. Kikuchi, S. Kitada, A. Ohno, S. Aramaki, S. Maenosono, Applied Physics Letters 92 (2008) 173307.

[8] A. Kumar, J. Prakash, D. S. Mehta, A. M. Biradar, W. Haase, Applied Physics Letters 95 (2009) 023117.

[9] H. Qi, T. Hegmann, Journal of Materials Chemistry 16 (2006) 4197.

[10] J. Prakash, A. Choudhary, A. Kumar, D. S. Mehta, A. M. Biradar, Applied Physics Letters 93 (2008) 112904.

[11] D. N. Chausov, A. D. Kurilov, R. N. Kucherov, A. V. Simakin, S. V. Gudkov, Journal of Physics: Condensed Matter 32 (2020) 395102.

[12] R. Bitar, G. Agez, M. Mitov, Soft Matter 7 (2011) 8198.

[13] A. Roy, B. P. Singh, G. Yadav, H. Khan, S. Kumar, A. Srivastava, R. Manohar, Journal of Molecular Liquids 295 (2019) 111872.

[14] B. P. Singh, S. Sikarwar, K. Agrahari, S. Tripathi, R. K. Gangwar, R. Manohar, K. K. Pandey, Journal of Molecular Liquids 325 (2021) 115172.

[15] M. Middha, R. Kumar, K. K. Raina, Liquid Crystals 43 (2016) 1002.

[16] S.-Y. Huang, C.-C. Peng, L.-W. Tu, C.-T. Kuo, Molecular Crystals and Liquid Crystals 507 (2009) 301.

[17] D. K. Pandey, U. B. Singh, R. Dhar, R. Dabrowski, M. B. Pandey, Phase Transitions 92 (2019) 931.

[18] X. Li, C. Yang, Q. Wang, D. Jia, L. Hu, Z. Peng, L. Xuan, Optics Communications 286 (2013) 224.

[19] U. B. Singh, R. Dhar, R. Dabrowski, M. B. Pandey, Liquid Crystals 40 (2013) 774.

[20] F. Simoni, O. Francescangeli, Y. Reznikov, S. Slussarenko, Optics Letters 22 (1997) 549.

[21] C. R. Lee, T. L. Fu, K. T. Cheng, T. S. Mo, A. Y. Fuh, Phys Rev E Stat Nonlin Soft Matter Phys 69 (2004) 031704.

[22] L. C. Lin, H. C. Jau, T. H. Lin, A. Y. Fuh, Opt Express 15 (2007) 2900.

[23] C. J. Hsu, B. P. Singh, M. Antony, P. Selvaraj, R. Manohar, C. Y. Huang, Optics Express 28 (2020) 22856.

[24] B. P. Singh, C.-Y. Huang, D. P. Singh, P. Palani, B. Duponchel, M. Sah, R. Manohar, K. K. Pandey, Journal of Molecular Liquids 325 (2021) 115130.

[25] C.-Y. Tang, S.-M. Huang, W. Lee, Journal of Physics D: Applied Physics 44 (2011) 355102.

[26] F.-C. Lin, P.-C. Wu, B.-R. Jian, W. Lee, Advances in Condensed Matter Physics 2013 (2013) 271574.

[27] J. Mirzaei, M. Urbanski, K. Yu, H.-S. Kitzerow, T. Hegmann, Journal of Materials Chemistry 21 (2011) 12710.

[28] A. Kumar, J. Prakash, A. D. Deshmukh, D. Haranath, P. Silotia, A. M. Biradar, Applied Physics Letters 100 (2012) 134101.

[29] H. Qi, T. Hegmann, Journal of Materials Chemistry 18 (2008) 3288.

[30] C.-Y. Huang, C.-Y. Hu, H.-C. Pan, K.-Y. Lo, Japanese Journal of Applied Physics 44 (2005) 8077.

[31] B. Coşkun, Journal of Molecular Structure 1191 (2019) 278.

[32] H.-M. Huang, E.-Y. Chuang, F.-L. Chen, J.-D. Lin, Y.-C. Hsiao, Polymers 12 (2020) 2294.

[33] I. Khoo, K. Chen, Y. Z. Williams, IEEE Journal of Selected Topics in Quantum Electronics 12 (2006) 443.

[34] P. Malik, A. Chaudhary, R. Mehra, K. K. Raina, Advances in Condensed Matter Physics 2012 (2012) 853160.

[35] X. Lu, H. Zhang, G. Fei, B. Yu, X. Tong, H. Xia, Y. Zhao, Advanced Materials 30 (2018) 1706597.

[36] T. A. Kandiel, L. Robben, A. Alkaim, D. Bahnemann, Photochemical & Photobiological Sciences 12 (2013) 602.

[37] J. S. Roy, T. Pal Majumder, R. Dabrowski, Journal of Molecular Structure 1098 (2015) 351.

[38] C. Y. Huang, P. Selvaraj, G. Senguttuvan, C. J. Hsu, Journal of Molecular Liquids 286 (2019) 110902.

[39] P.-C. Wu, S.-Y. Yang, W. Lee, Journal of Molecular Liquids 218 (2016) 150.

[40] H. Ayeb, S. Alaya, M. Derbali, L. Samet, J. Bennaceur, F. Jomni, T. Soltani, Liquid Crystals 48 (2021) 223.

[41] M. A. Mohamed, W. Salleh, J. Jaafar, N. Yusof, 2014.

[42] A. V. Ivashchenko, Dichroic dyes for liquid crystal displays. CRC Press, 1994.

[43] J. Y. Kim, H. S. Jung, J. H. No, J.-R. Kim, K. S. Hong, Journal of electroceramics 16 (2006) 447.

[44] K. H. Chen, W. Y. Chang, J. H. Chen, Opt Express 17 (2009) 14143.

[45] M. Schadt, Annu. Rev. Mater. Sci. 27 (1997) 305.

[46] B. P. Singh, G. Pathak, A. Roy, G. Hegde, P. K. Tripathi, A. Srivastava, R. Manohar, Liquid Crystals 46 (2019) 1808.

[47] D. Pauluth, K. Tarumi, Journal of Materials Chemistry 14 (2004) 1219.

[48] H. K. Shin, J.-H. Seo, T.-H. Yoon, J. C. Kim, H. S. Woo, S. T. Shin, Japanese Journal of Applied Physics 48 (2009) 111502.

[49] S.-W. Liao, C.-T. Hsieh, C.-C. Kuo, C.-Y. Huang, Applied Physics Letters 101 (2012) 161906.

[50] S. C. Jeng, S. J. Hwang, C. Y. Yang, Opt Lett 34 (2009) 455.

[51] Y. S. Ha, H. J. Kim, H. G. Park, D. S. Seo, Opt Express 20 (2012) 6448.

[52] M. Bharath Kumar, M. Awwal Adeshina, D. Kang, Y. Jee, T. Kim, M. Choi, J. Park, Nanomaterials (Basel) 10 (2020).

[53] S. Ishihara, M. Mizusaki, Journal of the Society for Information Display 28 (2020) 44.